Echocardiography Dedicated to Small Animal Models (Rodents) in Non-Ischemic Cardiomyopathies

André Timóteo Sapalo , Pedro De Oliveira Neto , Minna Moreira Dias Romano *

Posted Date: 20 May 2025

doi: 10.20944/preprints202505.1456.v1

Keywords: cardiomyopathies; echocardiography; animal models; speckle tracking echocardiography; myocardial remodeling; ventricular function; atrial function; heart failure ECHO: echocardiography

 doi:10.20944/preprints202505.1456.v1

Article

Echocardiography Dedicated to Small Animal Models (Rodents) in Non-Ischemic Cardiomyopathies

André Timóteo Sapalo, Pedro De Oliveira Neto and Minna Moreira Dias Romano *

Medical School of Ribeirao Preto – University of São Paulo, São Paulo, Brazil

* Correspondence: Minna Moreira Dias Romano, MD, PhD; Email: minna@fmrp.usp.br, Cardiology Division – Internal Medicine Department, Hospital das Clínicas, Faculdade de Medicina de Ribeirão Preto, 3900 Bandeirantes Avenue, Ribeirão Preto – São Paulo – Brazil; ZIP Code 14048900 Tel. +551636022599 – Fax. +551636330869

Abstract: This study emphasizes the importance of using tailored echocardiographic parameters for evaluating non-ischemic cardiomyopathies (NICs) in small animal (rodent) models. NICs can arise from conditions that cause pressure overload, such as aortic constriction and hypertension, or from volume overload due to impaired renal function and cardiometabolic disorders. In these cases, myocardial injury is typically secondary to extracardiac changes. Conversely, some models involve direct myocardial damage, such as those induced by cardiotoxic drugs or infectious agents, which are marked by acute myocardial edema and subsequent cardiomyocyte apoptosis. Echocardiographic assessment in these models often lacks standardization, leading to variability in data interpretation. To address this, the study proposes a comprehensive framework of echocardiographic parameters, including anatomical, geometric, and functional indices. Special attention is given to detecting reduced ventricular compliance and diastolic dysfunction, which are common features in these models. While ejection fraction is a traditional measure of systolic function, advanced techniques like speckle tracking echocardiography can reveal subclinical systolic dysfunction. The inclusion of parameters related to atrial overload and pulmonary congestion is also recommended. Overall, the study advocates for a standardized echocardiographic approach to enhance the accuracy and translational relevance of NIC research in preclinical animal models.

Keywords: cardiomyopathies; echocardiography; animal models; speckle tracking echocardiography; myocardial remodeling; ventricular function; atrial function; heart failure ECHO: echocardiography

1. Introduction

Echocardiography (ECHO) has become an essential technology, widely utilized by cardiologists and sonographers. It is an indispensable tool in diagnosing and following changes in several heart disease conditions in clinical and research settings. The effective use of echocardiography requires mastering a complex set of skills, which consists of two primary components: performing image acquisitions and interpreting image measures and function. Despite significant advances, echocardiography remains technique-dependent and demands significant training for physicians and sonographers. ECHO provides critical information on cardiac morphology, function, and hemodynamics in a noninvasive manner, making it the most frequently performed cardiovascular examination after electrocardiography and chest radiography [1]. In less than half a century, this technique has evolved into a cornerstone of cardiovascular medicine [2]. The historical evolution of echocardiography includes key developments such as M-mode, two-dimensional (2D) images, Doppler, Tissue Doppler, stress modalities, transesophageal, intraoperative, contrast, three-dimensional, and intracardiac echocardiography [3,4].

 doi:10.20944/preprints202505.1456.v1

Despite its substantial contributions to both clinical practice and biomedical research, echocardiography remains the only major medical imaging modality that has not been recognized with a Nobel Prize. While pioneers such as Edler and Hertz are acknowledged for their foundational work in cardiac imaging [5], the advancement of echocardiography has relied heavily on fundamental physics principles. Currently, ultrasound technology continues to evolve, not only through the integration of novel scientific discoveries but also via its expanding applications across a wide range of pathological conditions and in both invasive and surgical procedures.

Historically, the 1960s and 1970s marked the establishment of the first academic course in cardiac ultrasound, the publication of the first textbook on echocardiography, and the introduction of the term "echocardiography" [4,6–8]. With expanding applications and increasing portability of ECHO machines, this technology is expected to become even more widespread in clinical medicine, already evolving to pocket equipment with an intention to even substitute the stethoscope [9]. In animal models, still so useful in basic and translational science, the use of ECHO is relatively new [10], lacking significant historical milestones. However, its application in the evaluation of rodent models of cardiovascular diseases has grown, particularly due to the increasing availability of genetic models of several kinds of conditions [11], and it is continually evolving [12].

In this context, ECHO instrumentation for rodent models has improved, offering enhanced spatial and temporal resolution, leading to more accurate assessments of systolic and diastolic function parameters, as well as tissue characteristics of myocardium, extrapolating intracardiac pressures, as well as giving insights into microvascular [13]. The initial applications of ECHO in rodents involved the use of pediatric probes designed for human clinical equipment to study infant hearts adapted to small animals. Presently, there are only a limited number of manufacturers producing ultrasound equipment with cardiac probes specifically designed for small animals. The technique also faces another limitation, which is the lack of standardized protocols and minimum requirements to ensure a reliable and accurate assessment of cardiac function. A detailed description and standardization of methods for data acquisition and analysis would significantly enhance the value of studies performed in to study cardiac morphology and function in several conditions simulated in rodents [14–17]. Although recent literature has proposed suggestions and recommendations [18–21], it is crucial for researches to follow standardized protocols for the geometric and functional assessment of rodent ECHO[22]. Establishing well-defined and standardized echocardiographic conditions will facilitate the accurate evaluation of cardiac function data derived from small rodents, benefiting both researchers and reviewers.

This article will focus on compiling ECHO techniques dedicated to small animal models of non-ischemic cardiomyopathies, specifically for research in rodents. Emphasis will be placed on monitoring left ventricular (LV) geometry and function, as these are key elements in experimental studies aimed at understanding the pathophysiology of cardiac diseases and evaluating the potential therapeutic effects of innovative treatments.

2. Non-Ischemic Cardiomyopathy

Non-ischemic cardiomyopathy (NIC) refers to myocardial injury that leads to myocardial dysfunction (systolic or diastolic) and secondary consequences and ar not related to ischemic myocardial disease nor to systemic hypertension or valvopathies [23,24]. The etiologies of NIC are complex and multifactorial, encompassing drug toxicity, genetic diseases or predisposition, infectious diseases or inflammatory and immunological conditions, as well as deposit diseases [25]. In experimental animal models, NIC is commonly simulated using techniques such as transverse aortic constriction, a surgical procedure that induces heart failure (HF) due to pressure overload [26]. Additionally, cardiac hypertrophy and heart failure can be induced by infusion of angiotensin II [27] or isoproterenol [28]. In both scenarios, the disease induced is a kind of overload cardiomyopathy, similar to systemic arterial hypertension but not exactly secondary to direct myocardial aggression. In experimental animal models, toxic and infectious cardiomyopathies are characterized by myocardial edema in the acute phase, progressively accompanied by apoptosis. In models associated with metabolic comorbidities and pressure overload, myocardial remodeling involves cellular spacing and changes in collagen deposition, among other infiltrative alterations.

 doi:10.20944/preprints202505.1456.v1

In the group of these conditions of NIC, is also classified a not well-known disease still referred to as heart failure with preserved ejection fraction (HFpEF). Patients with HFpEF are usually female, with a group of comorbidities such as obesity, systemic hypertension, sedentarism, and glycemic metabolic disease. In rodents, hypertensive cardiomyopathy is studied through the use of genetically modified hypertension rats such as the spontaneously hypertensive rat [29]. Obesity is present in the Zucker rat strains [30] and is also recognized as a cardiac risk factor. Furthermore, models induced HF with reduced ejection fraction (HFrEF) by drug toxicity [31,32] such as those involving streptozotocin [33], dexamethasone [34], doxorrubicin [35], isoproterenol [36] as well as models induced by venom, including scorpion venom [37] are described. Another neglected disease endemic in all of Latin America, such as chronic cardiac Chagas disease, a parasitic-induced disease which still represents a challenge to cardiology, is now well-reproduced in a special rodent animal, the Syrian hamster [38]. In these models, echocardiography plays a critical role in evaluating both cardiac anatomical and functional changes, thereby validating and confirming the induction of heart disease [39] and intervention effects.. It is essential in distinguishing between adaptive and maladaptive remodeling processes [40]. However, sometimes, cardiac structural and functional changes observed in these models are nonspecific and overlap with common findings of various pathological conditions [41]. Also, some physiologic adaptations to overload such as the “athlete's heart” condition may present with geometrical and functional alterations able to be evaluated by ECHO and the technology may offer tools to differentiate cardiac remodeling typical of adaptations to overload conditions from pathological hypertrophy which adversely affects myocardial function [42,43].

3. The Role of Echocardiography in Assessing Cardiac Geometry

Myocardial remodeling is primarily influenced by the etiological factors underlying heart disease. In NIC conditions, pathological aggression can occur directly at the level of the cardiomyocyte, as observed in infectious etiologies, toxic, or inflammatory conditions, and even in genetic etiologies. Myocardial lesion is characterized by edema in early phases and progressive deterioration of the cardiomyocytes in the chronic phase [44], evolving to apoptosis and fibrosis. In heart disease models associated with pressure overload (systemic arterial hypertension, aorta constriction), a trigger to hypertrophy is predominant, secondary to increased afterload [45–48]. Early studies suggested that concentric left ventricular (LV) hypertrophy is indeed the main finding in experimental pressure overload models [49]. However, more recent research indicates that many pressure overload models exhibit geometric characteristics within the normal range, albeit with reduced ventricular compliance [50]. The probable explanation for this is the early myocardial collagen deposition and microstructural changes, such as those in the sarcoplasmic reticulum, which lead to increased ventricular tension and compromised LV distensibility [51]. Similarly, in metabolic heart diseases, but also associated with pressure overload secondary to arterial hypertension, cardiomyocytes tend to be thicker and less elongated compared to those in heart diseases that affect preload [52,53]. These findings may differ from the pathophysiology of reactive hypertrophy in isolated afterload increases, such as in hypertensive heart disease.

Indeed, reactive hypertrophy is also present in other kinds of myocardial direct aggression without afterload increment. In metabolic and inflammatory processes, such as obesity and dysglycemia, hypertrophy remodelling also occurs, probably related to other signalizations such as those involving cyclic GMP and oxidative stress mechanisms. Hypertrophy is frequently accompanied by microvascular dysfunction and also endothelial hypertrophy (citar a última referencia que discutimos e outras sobre HVE). Microvascular dysfunction may be documented by several methods in non-invasive methods, and with Echo, the study of coronary flow reserve may demonstrate not only macrovascular obstruction in ischemic models of cardiomyopathy, but also microvascular dysfunction in NIC.

In both conditions, whether those that increase myocardial fiber stretching or those that result in thicker, less elongated cardiomyocytes, ECHO can quantify chamber dimensions, extrapolate left ventricle mass and geometric pattern of remodeling, measuring relative thickness of LV walls [54].

Technically, bidimensional ECHO images are feasible in rodent models such as rats, mice, hamsters, and others, although parasternal (PE) views are preferred over apical views. Dedicated

 doi:10.20944/preprints202505.1456.v1

rodent machines offer high-resolution transducers (20-30 MHz), and if well acquired, the images have a very good resolution (Figure 1). Parasternal long axis view (PEL) allow quantification of left atrium (LA), left ventricle (LV) and wall thickness of interventricular septum and posterior wall (IVS and PW). The same structures of LV may be evaluated through parasternal short views (PES). Measurements of LV end diastolic and end systolic diameter may be performed from both views and also using M-Mode, which presents a better time resolution (Figure 1). LV mass is determined using the Devereux formula [54] and normalized to body weight. This widely accepted formula has been extensively utilized in rodents.

Although less used in basic and translational science, LA diameter and volumes may be measured from PEL and PES views, and the last one allows comparison with aortic diameter [55]. The Rishniw method, though less widely known, has been described in some experimental studies involving rodents. As demonstrated in the image, it is crucial to draw a line from the commissure between the non-coronary cusp and the right coronary cusp to the midpoint of the sinuses of Valsalva. The LA diameter is determined by tracing a line from the commissure between the non-coronary cusp and the left coronary cusp to the posterior wall of the LA. These two measurements are related through the LA/Ao ratio [56].

Some animal models of disease represent LV segmentation compromise not in a diffuse pattern, which is common in NIC, but in a segmental pattern, such as in Chagas' disease or Takotsubo, simulated by isoproterenol. Bidimensional (2D) ECHO images may also be used to evaluate LV segmental motion, using the wall motion segmental score similarly to human ischemic myocardial disease, with the difference to split LV in 13 segments, instead of the 17 we have in human ECHO (Figure 1). Segmentation allows analysis of wall motion abnormalities in a semiquantitative way [57] but also will allow regional deformation analysis as we will discuss later.

Although the segmental mobility index is commonly used in the context of impaired myocardial perfusion due to ischemic heart disease, it has also proven effective in analyzing myocardial segmental motion in certain experimental animal models [58]. Each LV segment will be classified based on wall motion in a scale typically ranging from 1-4, based on a qualitative assessment of regional function and systolic thickening, as described in Table 1. system, which also includes the identification of aneurysmal segments [59].

Table 1. Segmental mobility scale.

Score	Wall movement	Definition
1	Normal/hyperkinesia	Normal systolic movement and thickening
2	Hypokinesia	Reduced systolic motion or thickening
3	Acinese	Absence of systolic inward movement or thickening
4	Dyskinesia or Aneurysm	Paradoxical ("bulging") or outward movement

It is important to recognize that, in conditions of low compliance and myocardial hypertrophy, the internal ventricular diameter tends to decrease, and reduced compliance can lead to atrial overload. Consequently, the left atrium (LA) plays a critical role in facilitating the connection between the LV and the pulmonary circulation. This role allows the LV to function effectively as a conduit with controlled capacity, while protecting the pulmonary vasculature from fluctuations in LV pressure [60]. Therefore, the LA should be included in the hemodynamic measurements in rodent models, using both linear and volumetric assessments, as illustrated in **Figure 1**. The elliptical method, available in ultrasound equipment, and the linear Rishniw method are commonly used to measure the LA diameter in veterinary echocardiography (**Table 2**).

 doi:10.20944/preprints202505.1456.v1

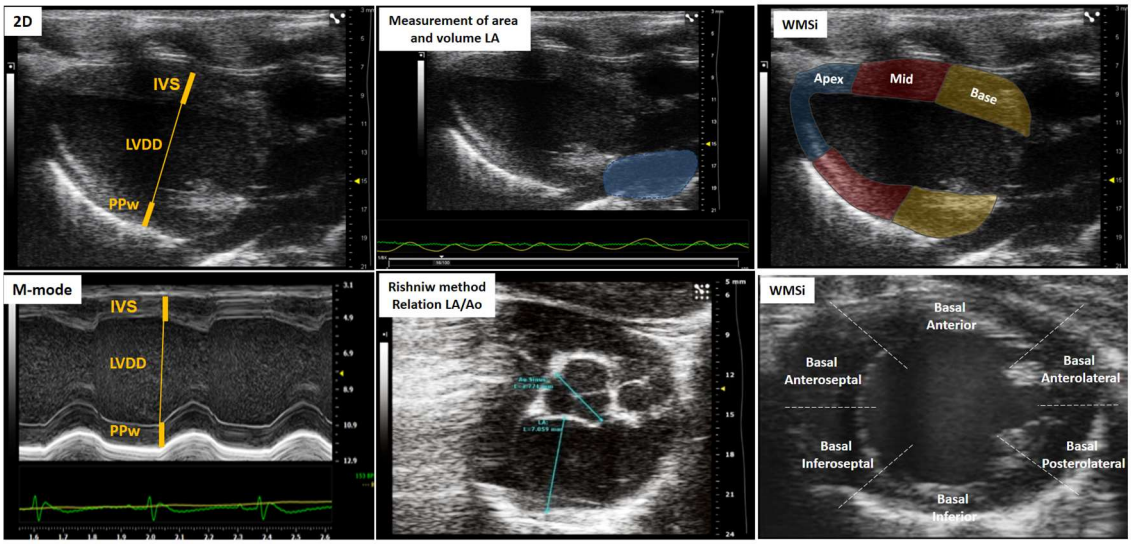

Figure 1. The parasternal long-axis (PEL) and short-axis (PES) views at the level of the papillary muscles are utilized for imaging. Both views allow visualization of the left ventricle (LV), right ventricle (RV), left atrium (LA), right atrium (RA), and the papillary muscles, enabling assessment of the anterior, posterior, inferior, and lateral segments. To acquire these images, position the transducer vertically in rodents, with the display facing the animal's head, which corresponds to the parasternal long-axis view. Then, rotate the transducer approximately 35° counterclockwise to obtain the parasternal short-axis view at the level of the papillary muscles.

Table 2. Variables ECHO of model.

Left atrium	Left ventricle	Right ventricle	Overload and congestion
LA volume	IVS	RV basal dimension	Pericardial effusion
LA-area	LVDD	(*Apical 4-chamber*)	B-lines (*Lulmonary congestion*)
LA-diameter	LVSD	Proximal dimension of the RV outflow tract	ICV collapsibility indices
Aort-Dimension	PPw	(*Parasternal short axis, anterior to the aortic valve*)	(*Animal breathing spontaneously*)
Relation LA/Ao	Relative thickness	Fractional area change RV	IVC distensibility indices
	LV mass	(*Apical 4-chamber*)	(*Animal on mechanical ventilation*)

LA, left atrium; IVS, interventricular septal thickness; LVDD, left ventricular end-diastolic diameter; LVPP, left ventricular posterior wall thickness; RV, right.

4. Role of Echocardiography in the Assessment of Left Ventricular Systolic Function

HF is commonly characterized by a reduction in left ventricular ejection fraction (LVEF), particularly in heart failure with reduced ejection fraction (HFrEF), which is often associated with ischemic heart disease and cardiomyocyte loss [61]. However, in non-ischemic cardiomyopathies, the clinical definition of HF accommodates the presence of preserved systemic function despite elevated filling pressures, as seen in HFpEF [62].

5. Evaluation of Pulmonary Congestion Using Lung Ultrasound in Rats

Cardiac disease will compromise LV function, and the diastolic dysfunction will be reproduced through increased LA pressures. Pressure overload can trigger pulmonary adaptations to increased

 doi:10.20944/preprints202505.1456.v1

postcapillary pressure. These adaptations include basement membrane thickening, enhanced alveolar fluid clearance, and increased lymphatic drainage [63,64]. This mechanism may result in congestion due to low compliance, often referred to as type 2 congestion or venocapillary congestion. This, in turn, activates the hypothalamic-pituitary-adrenal axis, stimulating reduced urinary output and promoting sodium retention [64–66]. Another factor contributing to fluid retention is the stimulation of natriuretic peptide (BNP) production into the LA with elevated pressures [67]. Elevated natriuresis may lead to disruptions in signaling at afferent sensory sites within the cardiopulmonary system [68]. These sites include impaired baroreceptors located in the carotid sinus and aortic arch, as well as malfunctioning mechanosensitive endings in cardiac chambers and the cardiopulmonary system, which may result in failure to detect elevations in circulating volume. This failure can contribute to congestion due to even more pressure overload and its associated cardiovascular outcomes [47,62,69].

In experimental animal models, the assessment of pulmonary congestion (PC) is primarily determined by the wet-to-dry weight ratio of the lung (W/D ratio). Lung tissue samples are typically weighed immediately after dissection (wet weight, W) and after being dried in an oven at 75°C for 48 hours (dry weight, D). The W/D ratio serves as a surrogate measure of water accumulation in the lung. This technique is usually performed as a terminal procedure, as it requires animal euthanasia to remove the lungs. To add to this scenario, lung ultrasound (LU) has gained increasing prominence in animal experimental settings, particularly for detecting the presence of multiple B-lines, commonly referred to as "comets," which move synchronously with the penetration of the ultrasound beam (if present). These B-lines are typically well-defined and appear as long, laser-like structures extending to the bottom of the screen without fading, reflecting fluid extravasation at the interstitial level [70] (Figure 2).

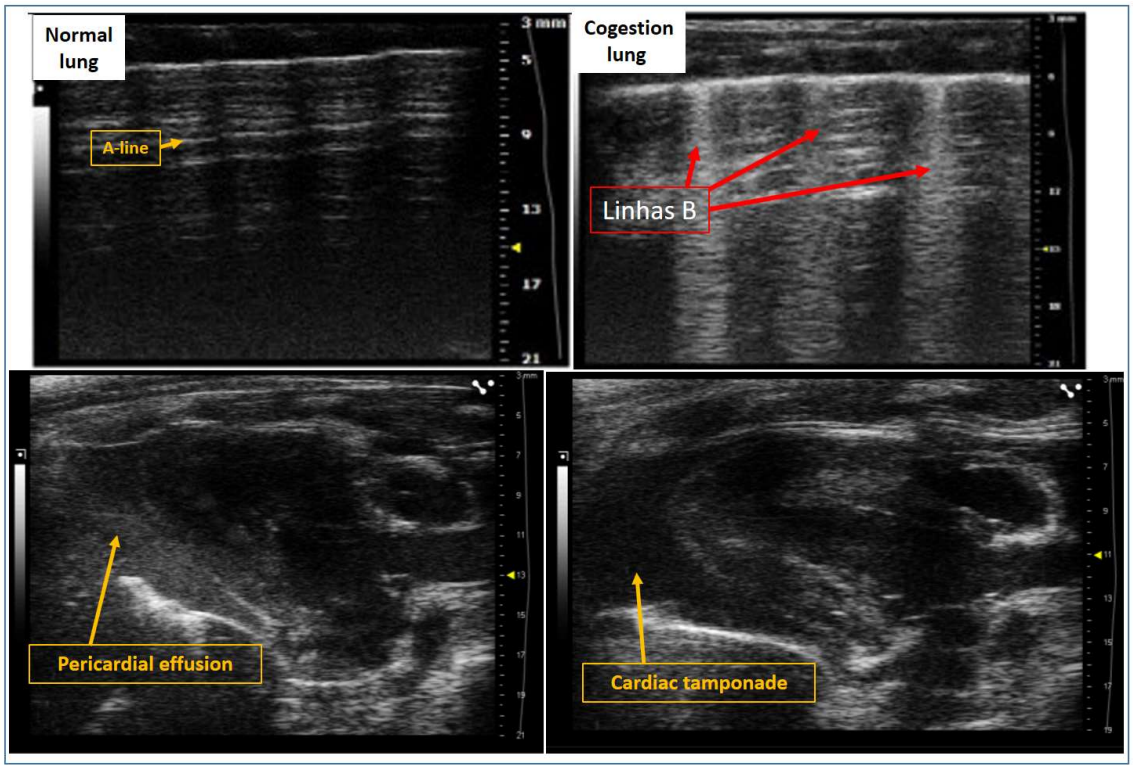

Figure 2. Lung ultrasound representation. The image illustrates a normal lung without congestion, indicated by A-lines, and a lung with pulmonary congestion, characterized by B-lines. Additionally, the figure includes ultrasound images of pericardial effusion and associated pathological findings in cases where the effusion is sufficiently severe to cause cardiac tamponade.

To assess the severity of pulmonary congestion, a LU scoring system has been developed to quantify the presence of A and B lines. Lines are defined as repetitive horizontal echogenic bands that are parallel to and originate from the pleural line, resulting from the predominance of air over

 doi:10.20944/preprints202505.1456.v1

fluid in the lung parenchyma. The presence of A lines is assigned a score of zero, indicating a normal LU pattern. B lines are described as discrete vertical hyperechoic reverberation artifacts. The B-line score is determined as follows: for each intercostal space, the number of B lines is counted (ranging from zero to ten, depending on the degree of signal confluence), and the percentage of the intercostal space occupied by B lines is calculated. This value is then divided by ten. A B-line count of 3–5 is classified as mild, 6–8 as moderate, and ≥8 as severe PC. This method has been shown to be increasingly effective compared to traditional assessments based solely on the W/D ratio. Additionally, this technique enables the monitoring of disease progression and therapeutic interventions without the need for euthanasia of animals to obtain lung samples.

6. Evaluation of RV Geometry and Function and its Association with Pulmonary Hypertension

Because of geometric difficulties in non-invasive methods, cardiac evaluation has traditionally focused almost exclusively on the LV, with the right ventricle (RV) often referred to in the literature as the "forgotten ventricle." However, the importance of RV function and physiology is well known as an essential determinant of prognosis in several scenarios. In recent years, the prognostic importance of the RV across various cardiovascular conditions has gained broader recognition [71–73]. Consequently, greater efforts have been directed toward incorporating RV assessment into routine clinical practice. Echocardiography is able to evaluate RV structure and function; however, conventional M-mode, two-dimensional, and Doppler-based assessments have recognized limitations [74]. Advanced techniques, such as three-dimensional (3D) echocardiography, Doppler tissue imaging (DTI), and speckle-tracking-based deformation imaging, have shown considerable promise and are increasingly applied in clinical settings [75]. Nonetheless, limited normative data and persistent technical challenges in RV imaging remain significant barriers.

A paradigm shift has occurred from purely visual assessment to the routine quantification of RV size and function. Unlike the LV, the RV possesses a complex geometry [76] and exhibits distinct pathophysiological responses to disease [77], complicating accurate quantification. As a result, some echocardiographers still rely on subjective visual estimates. Despite these difficulties, current best practices advocate for the inclusion of at least two quantitative RV metrics during transthoracic echocardiographic evaluation [78], as they provide valuable diagnostic and prognostic insights.

In experimental animal models, RV assessment should be integrated into standard imaging protocols and performed from multiple acoustic windows, including the PEL and right ventricular inflow and outflow views. Based on our team's experience, certain echocardiographic windows-particularly the apical four-chamber, apical RV-focused, and subcostal views-are challenging to obtain in rats but are more readily achievable in mice [79]. It is essential to ensure proper transducer alignment during image acquisition, especially in the apical four-chamber view, to avoid misestimation of RV size. In the context of HFpEF, the RV evaluation is not only important as a repercussion of elevated pulmonary pressures [80]. Emerging evidence suggests that coronary microvascular inflammation plays a central role in HFpEF pathophysiology [81], leading to more global myocardial remodeling, including in the RV [82]. Cardiomyocyte hypertrophy, characterized by increased cell diameter, is more pronounced in the presence of metabolic disorders and obesity [83], not solely in hypertensive conditions. Studies suggest that reduced activity of protein kinase G (PKG) is a key contributor to cardiac hypertrophy, promoting myocardial dysfunction through the hypophosphorylation of titin. PKG functions as a physiological brake on myocardial hypertrophy [84], a role supported by various experimental and clinical models. For example, in cultured neonatal rat cardiomyocytes, nitric oxide (NO) or cyclic guanosine monophosphate (cGMP) analogues attenuated norepinephrine-induced hypertrophy [85]. Similarly, in mice subjected to transverse aortic constriction, sildenafil, which enhances myocardial PKG signaling by inhibiting phosphodiesterase-5, prevented or reversed hypertrophy [86].

Recognition that myocardial remodeling in HFpEF is not confined to the LV necessitates consideration of pulmonary arterial hypertension (PAH) and its association with secondary tricuspid regurgitation (STR). The co-occurrence of PAH and STR is associated with adverse outcomes, though the mechanisms governing STR development remain incompletely understood. In human clinical

 doi:10.20944/preprints202505.1456.v1

science, a study by the Cleveland Clinic [87] suggests that RV geometry and function, rather than tricuspid valve anatomy, determine susceptibility to STR. Patients with STR exhibited greater RV dysfunction and more spherical RV morphology, as reflected by a higher sphericity index and reduced tricuspid annular plane systolic excursion (TAPSE), despite similar tricuspid annular and leaflet dimensions between groups.

In experimental rat models, echocardiographic visualization of the RV remains technically challenging. Nevertheless, when feasible, assessing tricuspid annular excursion through M-Mode (TAPSE) and tricuspid mitral annulus velocities good marker of function.

7. Conventional Assessment of LVEF in Rodent Models

In rodent models, LVEF is conventionally assessed via Echo, extrapolating LV volumes using either M-mode or two-dimensional (B-mode) imaging. M-mode echocardiography provides dimensional data to calculate both LVEF and fractional shortening (FS) [88,89], while the area-length method in B-mode imaging is employed to estimate end-diastolic and end-systolic volumes from area tracings (Figure 3).

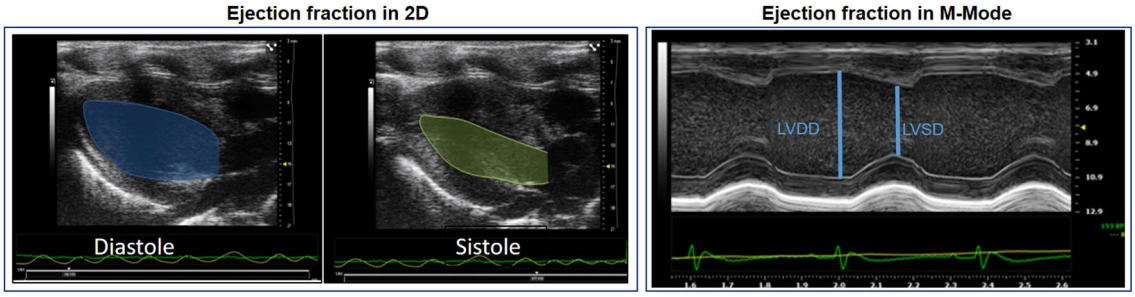

Figure 3. Assessment of left ventricular ejection fraction using two-dimensional (2D) echocardiography and M-mode imaging. Measurements include LV end-diastolic diameter (LVDD) and LV end-systolic diameter (LVSD), which are used to calculate ejection fraction as an index of global systolic function.

In addition to conventional assessment of ejection fraction, it is important to recognize that ejection fraction can also be estimated using myocardial deformation imaging. Longitudinal strain reflects the deformation of longitudinal myocardial fibers, which are predominantly located in the endocardial layer. Circumferential strain, on the other hand, measures the contraction of fibers oriented around the short axis of the ventricle. Radial strain, which reflects myocardial wall thickening, can be estimated through the combined analysis of longitudinal and circumferential deformation. Notably, circumferential and radial strain are more directly associated with left ventricular systolic performance, while longitudinal strain is more sensitive to early changes in isovolumetric contraction and subendocardial dysfunction (Figure 4).

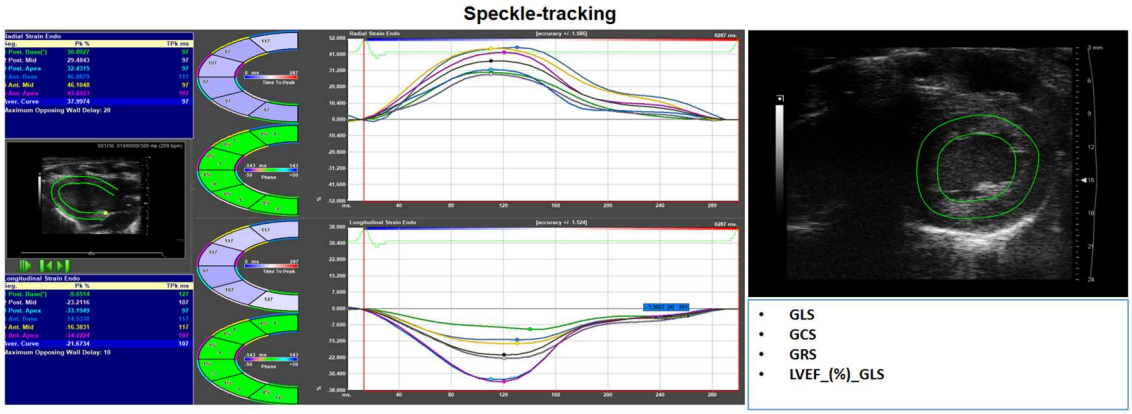

Figure 4. Analysis of myocardial deformation using speckle tracking echocardiography. This method enables the quantification of global longitudinal strain (GLS), global circumferential strain (GCS), and global radial strain

 doi:10.20944/preprints202505.1456.v1

(GRS), providing detailed assessment of myocardial mechanics. Additionally, left ventricular ejection fraction (LVEF) can be derived, offering a comprehensive evaluation of both global and regional systolic function.

Several studies have utilized mechanical models and in vivo animal experiments to better understand myocardial dysfunction in the presence of preserved LVEF, offering hypotheses to explain some paradoxical findings [90–92]. Evidence suggests that LVEF can be preserved or even overestimated (e.g., >60% in clinical settings) due to factors such as reduced ventricular compliance and increased myocardial density, particularly in hypertrophic conditions. While LVEF may remain within normal limits in many non-ischemic heart diseases, a diminished myocardial functional reserve has been observed under stress conditions, a phenomenon routinely assessed in human clinical cardiology using stress echocardiography [92–94].

Thus, considering preserved LVEF as preserved systolic function may be misleading. Importantly, LVEF reflects only the volumetric output during the systolic ejection phase and does not account for the isovolumetric contraction periods. Furthermore, LVEF estimation via bidimensional ECHO is based on geometric assumptions inherent to imaging techniques, which extrapolate volume from area measurements [95,96]. These limitations become particularly problematic in conditions with altered ventricular geometry or low-volume states, such as HFpEF, severe systemic arterial hypertension, aortic coarctation, or hypertrophic cardiomyopathies [92,97–99].

8. Advanced Assessment: Myocardial Deformation (Strain Imaging)

To more accurately characterize LV systolic functionmyocardial strain analysis using advanced ECHO techniques has become essential. Two-dimensional speckle tracking echocardiography (2D-STE) enables assessment of global and segmental myocardial deformation, independent of probe alignment withthe axis of deformation. In rodent models, strain measurements are commonly obtained from the PEL and PES views at the papillary muscle level (Figure 2).

The LV functions as both a pressure and volume pump during systole, and as a suction pump during diastole. LV systolic ejection involves complex deformation patterns, including longitudinal and circumferential shortening, radial thickening, and myocardial twisting. These are captured across different strain axis of deformation -longitudinal (GLS), circumferential (GCS), and radial (GRS) [100]. Still, when compounding basal and apical rotation of the LV torsion and twist can be measured [101].

Longitudinal mechanics are driven mainly by subendocardial fibers, while mid-myocardial fibers contribute primarily to circumferential and radial deformation [102]. During isovolumetric contraction, electrical activation begins at the endocardium, inducing a counterclockwise rotation of the LV base (from apical view) and clockwise rotation of the apex [103], culminating in torsion [104]. As activation spreads to the epicardial fibers located at a larger radius, the rotational direction reverses: the base rotates clockwise and the apex counterclockwise, optimizing ejection efficiency and enabling a greater myocyte shortening (15–20%) to generate a >55% reduction in LV volume [105]. Moreover, torsion couples systolic and diastolic function. During systole, stored mechanical energy is rapidly released as recoil during early diastole, facilitating efficient ventricular filling through active suction [106]. At the microscopic level, this corresponds to the rapid dissociation of actin-myosin cross-bridges and the reconfiguration of titin molecules to their resting state [100].

Using 2D-STE, it is possible the non-invasive measure these deformation parameters. The most clinically applied strain metrics, including GLS, GRS, and GCS, are still yet experimental. GLS and GCS are expressed as negative values (due to shortening), while GRS is positive (reflecting wall thickening). Torsion is expressed in degrees [102,107]. Although strain measurements are influenced by loading conditions, their sensitivity to preload and afterload is significantly less than that of LVEF, making them more reliable indicators of intrinsic myocardial contractility [108].

Strain imaging has demonstrated superior sensitivity to early myocardial dysfunction compared to LVEF, particularly in non-inflammatory cardiomyopathies affecting the mesocardium, such as Chagas disease, amyloidosis, and HFpEF [109,110]. In rodent models, GLS is measured from PEL, while circumferential and radial strain are measured from PES views, which is suitable for some

 doi:10.20944/preprints202505.1456.v1

artifacts of lateral resolution in the lateral image lobes. This issue does not affect GRS to the same extent, as it evaluates myocardial motion directed toward the cavity center and is less dependent on lateral resolution.

9. Role of Echocardiography in the Assessment of Left Ventricular Diastolic Function

Diastolic dysfunction, primarily resulting from impaired LV relaxation and reduced compliance, often precedes systolic dysfunction and is a hallmark of myocardial remodeling and hypertrophy. It frequently represents the earliest detectable manifestation of myocardial dysfunction in many cardiac heart diseases. The gold standard for the assessment of diastolic dysfunction remains the invasive measurement of increased LV filling pressures (EDP of LV) and time constant of relaxation (Tau). However, non-invasive estimation, especially in rodent models, remains technically challenging, even in clinical human practice [111].

ECHO evaluation of diastolic function in rats includes assessment of early (E wave) and late (A wave) mitral inflow velocities via pulsed-wave Doppler, and annular velocities (Em and Am) using DTI. The Doppler sample volume must be precisely aligned with blood flow direction, either at the mitral leaflet tips or lateral and septal annulus to avoid underestimation due to angle misalignment. Special attention to this detail is essential, as Doppler angle misalignment is a common source of measurement error in rodents [13].

- The **E wave represents** early diastolic filling driven by the pressure gradient between the left atrium and ventricle.
- The **A wave corresponds** to atrial contraction and the elastic recoil of the atrium and ventricle during late diastole.

The **E/A ratio** was one of the earliest indices used to characterize diastolic function [112,113].

Additional Doppler indices include:

- **Deceleration time (DT)** of the E wave, which correlates with mean left atrial pressure [114,115].
- **Mitral Annular Tissue Doppler Imaging (TDI)**

TDI is widely applicable in rodents due to the ease of tracking annular motion. The TDI waveform includes:

- A positive systolic wave (Sm), and
- Two negative diastolic waves: early (Em) and late (Am).

Unlike transmitral flow, annular TDI velocities are less sensitive to preload variations. The **E/Em ratio** serves as a non-invasive surrogate for LV filling pressure with a very good correlation to invasive measurements of elevated LA filling pressures [116,117] (**Figure 5**).

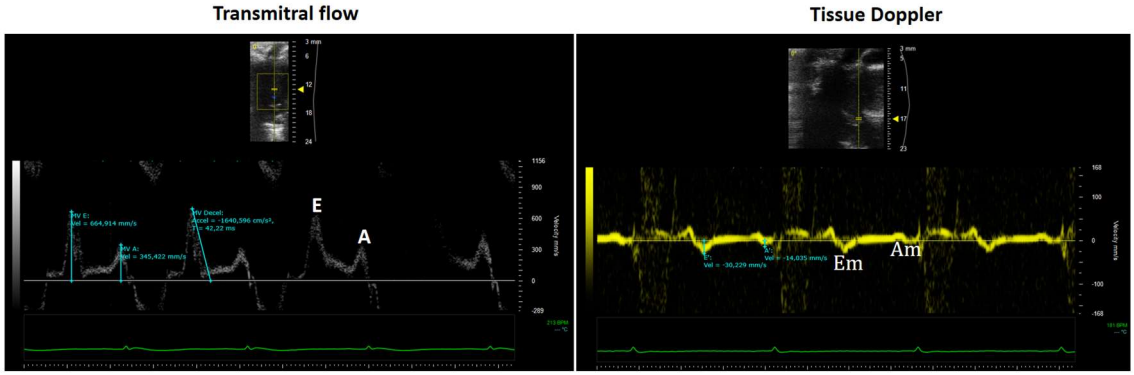

Figure 5. Assessment of transmitral flow using pulsed-wave Doppler, enabling evaluation of left ventricular (LV) diastolic filling. The E wave represents early passive filling, while the A wave reflects atrial contraction. Mitral annular motion is simultaneously assessed using tissue Doppler imaging (TDI), providing additional insight into diastolic function.

10. Coronary Flow Reserve Assessment in Non-Ischemic Models

 doi:10.20944/preprints202505.1456.v1

The capacity of the coronary circulation to autoregulate in response to variations in afterload and myocardial metabolic demands is a critical determinant of cardiac performance. One of the most accessible non-invasive methods for evaluating this physiological response is the assessment of coronary flow reserve (CFR) using Doppler echocardiography under pharmacological stimulation, typically with adenosine [118,119], as illustrated in **Figure 6**.

CFR represents the ratio of hyperemic to basal coronary blood flow and provides a functional measure of coronary microvascular integrity. Numerous NIC, particularly those characterized by myocardial hypertrophy, such as hypertensive cardiomyopathy and hypertrophic cardiomyopathy, are associated with a reduction in CFR [120,121]. This phenomenon reflects impaired vasodilatory capacity of the coronary microcirculation, which can precede overt myocardial dysfunction.

Emerging evidence suggests that myocardial remodeling leading to hypertrophy may originate at the vascular level, with subsequent parenchymal involvement. Vascular dysfunction is often mediated by oxidative stress, which disrupts endothelial function and alters vascular compliance, ultimately impairing myocardial perfusion, especially during periods of elevated metabolic demand [122,123].

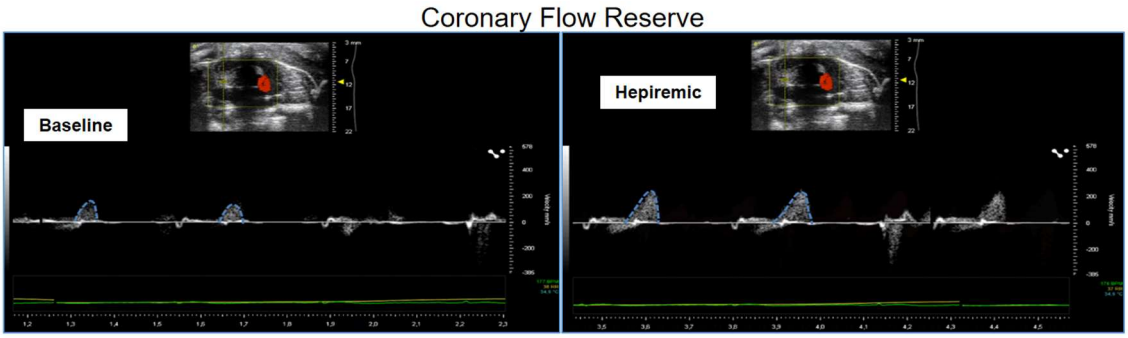

Figure 6. Assessment of coronary flow reserve (CFR) by Doppler echocardiography. Coronary flow velocity is measured at baseline and after pharmacological stress (e.g., adenosine or dobutamine), allowing evaluation of coronary microvascular function. CFR is calculated as the ratio of hyperemic to baseline diastolic flow velocity.

11. Challenges in Clinical and Experimental CFR Assessment

In human clinical practice, ECHO assessment of CFR remains limited by the technical challenge of imaging coronary arteries through standard transthoracic echocardiographic windows. As a result, CFR evaluation is not routinely included in conventional echocardiographic protocols. Instead, more advanced, expensive, and technically complex modalities such as myocardial perfusion scintigraphy, positron emission tomography, and cardiac magnetic resonance imaging are commonly employed when coronary microvascular function must be assessed. Notably, microvascular dysfunction has been increasingly recognized as a hallmark of some NIC, particularly in advanced disease stages and in patients with comorbidities such as systemic hypertension, obesity, and type 2 diabetes mellitus [124,125], as it is in HFpEF. These conditions are frequently associated with impaired CFR, even in the absence of significant epicardial coronary artery stenosis, underscoring the importance of microvascular health in the pathophysiology of NIC.

Abbreviations

NIC	Non-ischemic cardiomyopathy
HF	Heart failure
HFpEF	Heart failure preserved ejection fraction
LV	Left ventricular
IVS	Interventricular septal thickness
LVDD	Left ventricular end-diastolic diameter
LVPP	Left ventricular posterior wall thickness
LA	Left atrium
PC	Pulmonary congestion
BNP	Natriuretic peptide

 doi:10.20944/preprints202505.1456.v1

W/D ratio	wet-to-dry weight ratio of the lung
LU	Lung ultrasound
RV	Right Ventricle
3D	Three-dimensional
DTI	Doppler tissue imaging
ARVC	Arrhythmogenic right ventricular cardiomyopathy
PKG	Protein kinase G
NO	Nitric Oxide
cGMP	Cyclic guanosine monophosphate
PAH	pulmonary arterial hypertension
STR	Secondary tricuspid regurgitation
TAPSE	Tricuspid annular plane systolic excursion
LVEF	Left ventricular ejection fraction
HFrEF	Heart failure reduced ejection fraction
FS	Fractional shortening
2D-STE	Two-dimensional speckle tracking echocardiography
PEL	Parasternal long-axis
PES	Parasternal short-axis
GLS	Global longitudinal strain
GRS	Global radial strain
GCS	Global circumferential strain
Tau	time constant of relaxation
DT	Deceleration time
IVRT	Isovolumetric relaxation
TDI	Mitral annular tissue doppler imaging
CFR	Coronary flow reserve

References

1. Chang, A.; Cadaret, L.M.; Liu, K. Machine Learning in Electrocardiography and Echocardiography: Technological Advances in Clinical Cardiology. *Curr. Cardiol. Rep.* **2020**, *22*, 161, doi:10.1007/s11886-020-01416-9.
2. Izumo, M. Value of Echocardiography in the Treatment of Patients With Acute Heart Failure. *Front. Cardiovasc. Med.* **2021**, *8*, 740439, doi:10.3389/fcvm.2021.740439.
3. Gowda, R.M.; Khan, I.A.; Vasavada, B.C.; Sacchi, T.J.; Patel, R. History of the Evolution of Echocardiography. *Int. J. Cardiol.* **2004**, *97*, 1–6, doi:10.1016/j.ijcard.2003.07.018.
4. Feigenbaum, H. Evolution of Echocardiography. *Circulation* **1996**, *93*, 1321–1327, doi:10.1161/01.CIR.93.7.1321.
5. Singh, S.; Goyal, A. The Origin of Echocardiography: A Tribute to Inge Edler. *Tex. Heart Inst. J.* **2007**, *34*, 431–438.
6. Edler, I.; Lindström, K. The History of Echocardiography. *Ultrasound Med. Biol.* **2004**, *30*, 1565–1644, doi:10.1016/S0301-5629(99)00056-3.
7. Krishnamoorthy, V.K.; Sengupta, P.P.; Gentile, F.; Khandheria, B.K. History of Echocardiography and Its Future Applications in Medicine: *Crit. Care Med.* **2007**, *35*, S309–S313, doi:10.1097/01.CCM.0000270240.97375.DE.
8. Gillam, L.D.; Marcoff, L. Echocardiography: Past, Present, and Future. *Circ. Cardiovasc. Imaging* **2024**, *17*, doi:10.1161/CIRCIMAGING.124.016517.
9. Choi, B.G.; Mukherjee, M.; Dala, P.; Young, H.A.; Tracy, C.M.; Katz, R.J.; Lewis, J.F. Interpretation of Remotely Downloaded Pocket-Size Cardiac Ultrasound Images on a Web-Enabled Smartphone: Validation Against Workstation Evaluation. *J. Am. Soc. Echocardiogr.* **2011**, *24*, 1325–1330, doi:10.1016/j.echo.2011.08.007.
10. Reef, V.B. Advances in Echocardiography. *Vet. Clin. North Am. Equine Pract.* **1991**, *7*, 435–450, doi:10.1016/S0749-0739(17)30508-4.
11. Ram, R.; Mickelsen, D.M.; Theodoropoulos, C.; Blaxall, B.C. New Approaches in Small Animal Echocardiography: Imaging the Sounds of Silence. *Am. J. Physiol.-Heart Circ. Physiol.* **2011**, *301*, H1765–H1780, doi:10.1152/ajpheart.00559.2011.

 doi:10.20944/preprints202505.1456.v1

12. Zeng, Y.; Sun, X.; Zhang, J.; Chang, C.-F.; Liu, B.; Gong, C.; Ji, J.; Zhang, B.Z.; Wang, Y.; Xinhu Ren, M.; et al. High-Frequency Wearable Ultrasound Array Belt for Small Animal Echocardiography. *IEEE Trans. Ultrason. Ferroelectr. Freq. Control* **2024**, *71*, 1915–1923, doi:10.1109/TUFFC.2024.3492197.
13. Zacchigna, S.; Paldino, A.; Falcão-Pires, I.; Daskalopoulos, E.P.; Dal Ferro, M.; Vodret, S.; Lesizza, P.; Cannatà, A.; Miranda-Silva, D.; Lourenço, A.P.; et al. Towards Standardization of Echocardiography for the Evaluation of Left Ventricular Function in Adult Rodents: A Position Paper of the ESC Working Group on Myocardial Function. *Cardiovasc. Res.* **2021**, *117*, 43–59, doi:10.1093/cvr/cvaa110.
14. Jabs, M.; Rose, A.J.; Lehmann, L.H.; Taylor, J.; Moll, I.; Sijmonsma, T.P.; Herberich, S.E.; Sauer, S.W.; Poschet, G.; Federico, G.; et al. Inhibition of Endothelial Notch Signaling Impairs Fatty Acid Transport and Leads to Metabolic and Vascular Remodeling of the Adult Heart. *Circulation* **2018**, *137*, 2592–2608, doi:10.1161/CIRCULATIONAHA.117.029733.
15. Ong, S.-G.; Lee, W.H.; Huang, M.; Dey, D.; Kodo, K.; Sanchez-Freire, V.; Gold, J.D.; Wu, J.C. Cross Talk of Combined Gene and Cell Therapy in Ischemic Heart Disease: Role of Exosomal MicroRNA Transfer. *Circulation* **2014**, *130*, doi:10.1161/CIRCULATIONAHA.113.007917.
16. Wang, H.; Xu, X.; Fassett, J.; Kwak, D.; Liu, X.; Hu, X.; Falls, T.J.; Bell, J.C.; Li, H.; Bitterman, P.; et al. Double-Stranded RNA–Dependent Protein Kinase Deficiency Protects the Heart From Systolic Overload-Induced Congestive Heart Failure. *Circulation* **2014**, *129*, 1397–1406, doi:10.1161/CIRCULATIONAHA.113.002209.
17. Boon, R.A.; Iekushi, K.; Lechner, S.; Seeger, T.; Fischer, A.; Heydt, S.; Kaluza, D.; Tréguer, K.; Carmona, G.; Bonauer, A.; et al. MicroRNA-34a Regulates Cardiac Ageing and Function. *Nature* **2013**, *495*, 107–110, doi:10.1038/nature11919.
18. Lindsey, M.L.; Bolli, R.; Canty, J.M.; Du, X.-J.; Frangogiannis, N.G.; Frantz, S.; Gourdie, R.G.; Holmes, J.W.; Jones, S.P.; Kloner, R.A.; et al. Guidelines for Experimental Models of Myocardial Ischemia and Infarction. *Am. J. Physiol.-Heart Circ. Physiol.* **2018**, *314*, H812–H838, doi:10.1152/ajpheart.00335.2017.
19. Lindsey, M.L.; Kassiri, Z.; Virag, J.A.I.; De Castro Brás, L.E.; Scherrer-Crosbie, M. Guidelines for Measuring Cardiac Physiology in Mice. *Am. J. Physiol.-Heart Circ. Physiol.* **2018**, *314*, H733–H752, doi:10.1152/ajpheart.00339.2017.
20. Pachon, R.E.; Scharf, B.A.; Vatner, D.E.; Vatner, S.F. Best Anesthetics for Assessing Left Ventricular Systolic Function by Echocardiography in Mice. *Am. J. Physiol.-Heart Circ. Physiol.* **2015**, *308*, H1525–H1529, doi:10.1152/ajpheart.00890.2014.
21. Donner, D.G.; Kiriazis, H.; Du, X.-J.; Marwick, T.H.; McMullen, J.R. Improving the Quality of Preclinical Research Echocardiography: Observations, Training, and Guidelines for Measurement. *Am. J. Physiol.-Heart Circ. Physiol.* **2018**, *315*, H58–H70, doi:10.1152/ajpheart.00157.2018.
22. Tanaka, D.M.; Romano, M.M.D.; Carvalho, E.E.V.; Oliveira, L.F.L.; Souza, H.C.D.; Maciel, B.C.; Salgado, H.C.; Fazan-Júnior, R.; Simões, M.V. Effect of Different Anesthetic Agents on Left Ventricular Systolic Function Assessed by Echocardiography in Hamsters. *Braz. J. Med. Biol. Res.* **2016**, *49*, e5294, doi:10.1590/1414-431x20165294.
23. Manzi, L.; Buongiorno, F.; Narciso, V.; Florimonte, D.; Forzano, I.; Castiello, D.S.; Sperandeo, L.; Paolillo, R.; Verde, N.; Spinelli, A.; et al. Acute Heart Failure and Non-Ischemic Cardiomyopathies: A Comprehensive Review and Critical Appraisal. *Diagnostics* **2025**, *15*, 540, doi:10.3390/diagnostics15050540.
24. Barja, N.; Rozado, J.; Martín, M. Ischemic or Nonischemic Cardiomyopathy? *JACC Heart Fail.* **2019**, *7*, 995, doi:10.1016/j.jchf.2019.08.013.
25. Wang, Y.; Jia, H.; Song, J. Accurate Classification of Non-Ischemic Cardiomyopathy. *Curr. Cardiol. Rep.* **2023**, *25*, 1299–1317, doi:10.1007/s11886-023-01944-0.
26. Zhou, Q.; Kesteven, S.; Wu, J.; Aidery, P.; Gawaz, M.; Gramlich, M.; Feneley, M.P.; Harvey, R.P. Pressure Overload by Transverse Aortic Constriction Induces Maladaptive Hypertrophy in a Titin-Truncated Mouse Model. *BioMed Res. Int.* **2015**, *2015*, 1–6, doi:10.1155/2015/163564.
27. Tsukamoto, Y.; Mano, T.; Sakata, Y.; Ohtani, T.; Takeda, Y.; Tamaki, S.; Omori, Y.; Ikeya, Y.; Saito, Y.; Ishii, R.; et al. A Novel Heart Failure Mice Model of Hypertensive Heart Disease by Angiotensin II Infusion, Nephrectomy, and Salt Loading. *Am. J. Physiol.-Heart Circ. Physiol.* **2013**, *305*, H1658–H1667, doi:10.1152/ajpheart.00349.2013.

 doi:10.20944/preprints202505.1456.v1

28. Carll, A.P.; Willis, M.S.; Lust, R.M.; Costa, D.L.; Farraj, A.K. Merits of Non-Invasive Rat Models of Left Ventricular Heart Failure. *Cardiovasc. Toxicol.* **2011**, *11*, 91–112, doi:10.1007/s12012-011-9103-5.
29. Doris, P.A. Genetics of Hypertension: An Assessment of Progress in the Spontaneously Hypertensive Rat. *Physiol. Genomics* **2017**, *49*, 601–617, doi:10.1152/physiolgenomics.00065.2017.
30. Fredersdorf, S.; Thumann, C.; Ulucan, C.; Griese, D.P.; Luchner, A.; Riegger, G.A.J.; Kromer, E.P.; Weil, J. Myocardial Hypertrophy and Enhanced Left Ventricular Contractility in Zucker Diabetic Fatty Rats. *Cardiovasc. Pathol.* **2004**, *13*, 11–19, doi:10.1016/S1054-8807(03)00109-1.
31. Su, H.; Gorodny, N.; Gomez, L.F.; Gangadharmath, U.; Mu, F.; Chen, G.; Walsh, J.C.; Szardenings, K.; Kolb, H.C.; Tamarappoo, B. Noninvasive Molecular Imaging of Apoptosis in a Mouse Model of Anthracycline-Induced Cardiotoxicity. *Circ. Cardiovasc. Imaging* **2015**, *8*, doi:10.1161/CIRCIMAGING.114.001952.
32. Leerink, J.M.; Van De Ruit, M.; Feijen, E.A.M.; Kremer, L.C.M.; Mavinkurve-Groothuis, A.M.C.; Pinto, Y.M.; Creemers, E.E.; Kok, W.E.M. Extracellular Matrix Remodeling in Animal Models of Anthracycline-Induced Cardiomyopathy: A Meta-Analysis. *J. Mol. Med.* **2021**, *99*, 1195–1207, doi:10.1007/s00109-021-02098-8.
33. Furman, B.L. Streptozotocin-Induced Diabetic Models in Mice and Rats. *Curr. Protoc.* **2021**, *1*, e78, doi:10.1002/cpz1.78.
34. Gounarides, J.S.; Korach-André, M.; Killary, K.; Argentieri, G.; Turner, O.; Laurent, D. Effect of Dexamethasone on Glucose Tolerance and Fat Metabolism in a Diet-Induced Obesity Mouse Model. *Endocrinology* **2008**, *149*, 758–766, doi:10.1210/en.2007-1214.
35. O'Connell, J.L.; Romano, M.M.D.; Campos Pulici, E.C.; Carvalho, E.E.V.; De Souza, F.R.; Tanaka, D.M.; Maciel, B.C.; Salgado, H.C.; Fazan-Júnior, R.; Rossi, M.A.; et al. Short-Term and Long-Term Models of Doxorubicin-Induced Cardiomyopathy in Rats: A Comparison of Functional and Histopathological Changes. *Exp. Toxicol. Pathol.* **2017**, *69*, 213–219, doi:10.1016/j.etp.2017.01.004.
36. Campos, E.C.; Romano, M.M.D.; Prado, C.M.; Rossi, M.A. Isoproterenol Induces Primary Loss of Dystrophin in Rat Hearts: Correlation with Myocardial Injury. *Int. J. Exp. Pathol.* **2008**, *89*, 367–381, doi:10.1111/j.1365-2613.2008.00604.x.
37. Ouanes-Besbes, L.; El Atrous, S.; Nouira, S.; Aubrey, N.; Carayon, A.; El Ayeb, M.; Abroug, F. Direct vs. Mediated Effects of Scorpion Venom: An Experimental Study of the Effects of a Second Challenge with Scorpion Venom. *Intensive Care Med.* **2005**, *31*, 441–446, doi:10.1007/s00134-005-2555-y.
38. Ramirez, L.E.; Lages-Silva, E.; Soares Junior, J.M.; Chapadeiro, E. The Hamster (Mesocricetus Auratus) as Experimental Model in Chagas' Disease: Parasitological and Histopathological Studies in Acute and Chronic Phases of Trypanosoma Cruzi Infection. *Rev. Soc. Bras. Med. Trop.* **1994**, *27*, 163–169, doi:10.1590/S0037-86821994000300007.
39. Scherrer-Crosbie, M.; Thibault, H.B. Echocardiography in Translational Research: Of Mice and Men. *J. Am. Soc. Echocardiogr.* **2008**, *21*, 1083–1092, doi:10.1016/j.echo.2008.07.001.
40. Litwin, S.E.; Katz, S.E.; Weinberg, E.O.; Lorell, B.H.; Aurigemma, G.P.; Douglas, P.S. Serial Echocardiographic-Doppler Assessment of Left Ventricular Geometry and Function in Rats With Pressure-Overload Hypertrophy: Chronic Angiotensin-Converting Enzyme Inhibition Attenuates the Transition to Heart Failure. *Circulation* **1995**, *91*, 2642–2654, doi:10.1161/01.CIR.91.10.2642.
41. Abduch, M.C.D.; Assad, R.S.; Mathias Jr., W.; Aiello, V.D. The Echocardiography in the Cardiovascular Laboratory: A Guide to Research with Animals. *Arq. Bras. Cardiol.* **2013**, doi:10.5935/abc.20130239.
42. Flanagan, H.; Cooper, R.; George, K.P.; Augustine, D.X.; Malhotra, A.; Paton, M.F.; Robinson, S.; Oxborough, D. The Athlete's Heart: Insights from Echocardiography. *Echo Res. Pract.* **2023**, *10*, 15, doi:10.1186/s44156-023-00027-8.
43. Kovács, A.; Oláh, A.; Lux, Á.; Mátyás, C.; Németh, B.T.; Kellermayer, D.; Ruppert, M.; Török, M.; Szabó, L.; Meltzer, A.; et al. Strain and Strain Rate by Speckle-Tracking Echocardiography Correlate with Pressure-Volume Loop-Derived Contractility Indices in a Rat Model of Athlete's Heart. *Am. J. Physiol.-Heart Circ. Physiol.* **2015**, *308*, H743–H748, doi:10.1152/ajpheart.00828.2014.
44. Manca, P.; Nuzzi, V.; Cannatà, A.; Merlo, M.; Sinagra, G. Contemporary Etiology and Prognosis of Dilated Non-Ischemic Cardiomyopathy. *Minerva Cardiol. Angiol.* **2022**, *70*, doi:10.23736/S2724-5683.21.05736-7.

 doi:10.20944/preprints202505.1456.v1

45. Kim, J.H.; Jiang, Y.-P.; Cohen, I.S.; Lin, R.Z.; Mathias, R.T. Pressure-Overload-Induced Angiotensin-Mediated Early Remodeling in Mouse Heart. *PLOS ONE* **2017**, *12*, e0176713, doi:10.1371/journal.pone.0176713.
46. Merino, D.; Gil, A.; Gómez, J.; Ruiz, L.; Llano, M.; García, R.; Hurlé, M.A.; Nistal, J.F. Experimental Modelling of Cardiac Pressure Overload Hypertrophy: Modified Technique for Precise, Reproducible, Safe and Easy Aortic Arch Banding-Debanding in Mice. *Sci. Rep.* **2018**, *8*, 3167, doi:10.1038/s41598-018-21548-x.
47. Crandall, D.L.; Goldstein, B.M.; Lizzo, F.H.; Lozito, R.J.; Cervoni, P. Development of an Animal Model for Investigating Disparate Myocardial Effects of Obesity and Hypertension. *J. Appl. Physiol.* **1988**, *64*, 1094–1097, doi:10.1152/jappl.1988.64.3.1094.
48. Frohlich, E.D.; Susic, D. Pressure Overload. *Heart Fail. Clin.* **2012**, *8*, 21–32, doi:10.1016/j.hfc.2011.08.005.
49. Sen, S. Regression of Cardiac Hypertrophy Experimental Animal Model. *Am. J. Med.* **1983**, *75*, 87–93, doi:10.1016/0002-9343(83)90124-9.
50. Katz, A.M.; Rolett, E.L. Heart Failure: When Form Fails to Follow Function. *Eur. Heart J.* **2016**, *37*, 449–454, doi:10.1093/eurheartj/ehv548.
51. Kai, H.; Kuwahara, F.; Tokuda, K.; Imaizumi, T. Diastolic Dysfunction in Hypertensive Hearts: Roles of Perivascular Inflammation and Reactive Myocardial Fibrosis. *Hypertens. Res.* **2005**, *28*, 483–490, doi:10.1291/hypres.28.483.
52. Leite-Moreira, A. Afterload Induced Changes in Myocardial Relaxation A Mechanism for Diastolic Dysfunction. *Cardiovasc. Res.* **1999**, *43*, 344–353, doi:10.1016/S0008-6363(99)00099-1.
53. Hassan, A.; Samaan, K.; Asfour, A.; Baghdady, Y.; Samaan, A.A. Ventricular Remodeling and Hemodynamic Changes in Heart Failure Patients with Non-Ischemic Dilated Cardiomyopathy Following Dapagliflozin Initiation. *Egypt. Heart J.* **2024**, *76*, 76, doi:10.1186/s43044-024-00508-z.
54. Devereux, R.B.; De Simone, G.; Ganau, A.; Koren, M.J.; Mensah, G.A.; Roman, M.J. Left Ventricular Hypertrophy and Hypertension. *Clin. Exp. Hypertens.* **1993**, *15*, 1025–1032, doi:10.3109/10641969309037090.
55. Medrano, G.; Hermosillo-Rodriguez, J.; Pham, T.; Granillo, A.; Hartley, C.J.; Reddy, A.; Osuna, P.M.; Entman, M.L.; Taffet, G.E. Left Atrial Volume and Pulmonary Artery Diameter Are Noninvasive Measures of Age-Related Diastolic Dysfunction in Mice. *J. Gerontol. A. Biol. Sci. Med. Sci.* **2016**, *71*, 1141–1150, doi:10.1093/gerona/glv143.
56. Rishniw, M.; Erb, H.N. Evaluation of Four 2-Dimensional Echocardiographic Methods of Assessing Left Atrial Size in Dogs. *J. Vet. Intern. Med.* **2000**, *14*, 429, doi:10.1892/0891-6640(2000)014<0429:EOFEMO>2.3.CO;2.
57. Teichholz, L.E.; Kreulen, T.; Herman, M.V.; Gorlin, R. Problems in Echocardiographic Volume Determinations: Echocardiographic-Angiographic Correlations in the Presence or Absence of Asynergy. *Am. J. Cardiol.* **1976**, *37*, 7–11, doi:10.1016/0002-9149(76)90491-4.
58. Tanaka, D.M.; O'Connell, J.L.; Fabricio, C.G.; Romano, M.M.D.; Campos, E.C.; Oliveira, L.F.L.D.; Schmidt, A.; Carvalho, E.E.V.D.; Simões, M.V. Efficacy of Different Cumulative Doses of Doxorubicin in the Induction of a Dilated Cardiomyopathy Model in Rats. *ABC Heart Fail. Cardiomyopathy* **2022**, *2*, 242–249, doi:10.36660/abchf.20220074.
59. Lang, R.M.; Badano, L.P.; Mor-Avi, V.; Afilalo, J.; Armstrong, A.; Ernande, L.; Flachskampf, F.A.; Foster, E.; Goldstein, S.A.; Kuznetsova, T.; et al. Recommendations for Cardiac Chamber Quantification by Echocardiography in Adults: An Update from the American Society of Echocardiography and the European Association of Cardiovascular Imaging. *J. Am. Soc. Echocardiogr.* **2015**, *28*, 1-39.e14, doi:10.1016/j.echo.2014.10.003.
60. Rossi, A.; Gheorghiade, M.; Triposkiadis, F.; Solomon, S.D.; Pieske, B.; Butler, J. Left Atrium in Heart Failure With Preserved Ejection Fraction: Structure, Function, and Significance. *Circ. Heart Fail.* **2014**, *7*, 1042–1049, doi:10.1161/CIRCHEARTFAILURE.114.001276.
61. Bozkurt, B.; Coats, A.J.S.; Tsutsui, H.; Abdelhamid, C.M.; Adamopoulos, S.; Albert, N.; Anker, S.D.; Atherton, J.; Böhm, M.; Butler, J.; et al. Universal Definition and Classification of Heart Failure: A Report of the Heart Failure Society of America, Heart Failure Association of the European Society of Cardiology, Japanese Heart Failure Society and Writing Committee of the Universal Definition of Heart Failure: Endorsed by the Canadian Heart Failure Society, Heart Failure Association of India, Cardiac Society of

 doi:10.20944/preprints202505.1456.v1

Australia and New Zealand, and Chinese Heart Failure Association. *Eur. J. Heart Fail.* **2021**, *23*, 352–380, doi:10.1002/ejhf.2115.

62. Conceição, G.; Heinonen, I.; Lourenço, A.P.; Duncker, D.J.; Falcão-Pires, I. Animal Models of Heart Failure with Preserved Ejection Fraction. *Neth. Heart J.* **2016**, *24*, 275–286, doi:10.1007/s12471-016-0815-9.
63. Parker, J.C.; Townsley, M.I. Evaluation of Lung Injury in Rats and Mice. *Am. J. Physiol.-Lung Cell. Mol. Physiol.* **2004**, *286*, L231–L246, doi:10.1152/ajplung.00049.2003.
64. Pacher, P.; Nagayama, T.; Mukhopadhyay, P.; Bátkai, S.; Kass, D.A. Measurement of Cardiac Function Using Pressure–Volume Conductance Catheter Technique in Mice and Rats. *Nat. Protoc.* **2008**, *3*, 1422–1434, doi:10.1038/nprot.2008.138.
65. Corrigendum to: Heart Failure with Preserved Ejection Fraction in Humans and Mice: Embracing Clinical Complexity in Mouse Models. *Eur. Heart J.* **2022**, *43*, 1940–1940, doi:10.1093/eurheartj/ehab883.
66. Picchi, M.G.; Mattos, A.M.D.; Barbosa, M.R.; Duarte, C.P.; Gandini, M.D.A.; Portari, G.V.; Jordão, A.A. A High-Fat Diet as a Model of Fatty Liver Disease in Rats. *Acta Cir. Bras.* **2011**, *26*, 25–30, doi:10.1590/S0102-86502011000800006.
67. Speakman, J.R. Use of High-Fat Diets to Study Rodent Obesity as a Model of Human Obesity. *Int. J. Obes.* **2019**, *43*, 1491–1492, doi:10.1038/s41366-019-0363-7.
68. Kasiske, B.L.; O'Donnell, M.P.; Keane, W.F. The Zucker Rat Model of Obesity, Insulin Resistance, Hyperlipidemia, and Renal Injury. *Hypertension* **1992**, *19*, doi:10.1161/01.HYP.19.1_Suppl.I110.
69. Regan, J.A.; Mauro, A.G.; Carbone, S.; Marchetti, C.; Gill, R.; Mezzaroma, E.; Valle Raleigh, J.; Salloum, F.N.; Van Tassell, B.W.; Abbate, A.; et al. A Mouse Model of Heart Failure with Preserved Ejection Fraction Due to Chronic Infusion of a Low Subpressor Dose of Angiotensin II. *Am. J. Physiol.-Heart Circ. Physiol.* **2015**, *309*, H771–H778, doi:10.1152/ajpheart.00282.2015.
70. Ma, H.; Huang, D.; Zhang, M.; Huang, X.; Ma, S.; Mao, S.; Li, W.; Chen, Y.; Guo, L. Lung Ultrasound Is a Reliable Method for Evaluating Extravascular Lung Water Volume in Rodents. *BMC Anesthesiol.* **2015**, *15*, 162, doi:10.1186/s12871-015-0146-1.
71. Ghio, S.; Gavazzi, A.; Campana, C.; Inserra, C.; Klersy, C.; Sebastiani, R.; Arbustini, E.; Recusani, F.; Tavazzi, L. Independent and Additive Prognostic Value of Right Ventricular Systolic Function and Pulmonary Artery Pressure in Patients with Chronic Heart Failure. *J. Am. Coll. Cardiol.* **2001**, *37*, 183–188, doi:10.1016/S0735-1097(00)01102-5.
72. Haddad, F.; Doyle, R.; Murphy, D.J.; Hunt, S.A. Right Ventricular Function in Cardiovascular Disease, Part II: Pathophysiology, Clinical Importance, and Management of Right Ventricular Failure. *Circulation* **2008**, *117*, 1717–1731, doi:10.1161/CIRCULATIONAHA.107.653584.
73. Gorter, T.M.; Hoendermis, E.S.; Van Veldhuisen, D.J.; Voors, A.A.; Lam, C.S.P.; Geelhoed, B.; Willems, T.P.; Van Melle, J.P. Right Ventricular Dysfunction in Heart Failure with Preserved Ejection Fraction: A Systematic Review and Meta-analysis. *Eur. J. Heart Fail.* **2016**, *18*, 1472–1487, doi:10.1002/ejhf.630.
74. Longobardo, L.; Suma, V.; Jain, R.; Carerj, S.; Zito, C.; Zwicke, D.L.; Khandheria, B.K. Role of Two-Dimensional Speckle-Tracking Echocardiography Strain in the Assessment of Right Ventricular Systolic Function and Comparison with Conventional Parameters. *J. Am. Soc. Echocardiogr.* **2017**, *30*, 937-946.e6, doi:10.1016/j.echo.2017.06.016.
75. Addetia, K.; Miyoshi, T.; Amuthan, V.; Citro, R.; Daimon, M.; Gutierrez Fajardo, P.; Kasliwal, R.R.; Kirkpatrick, J.N.; Monaghan, M.J.; Muraru, D.; et al. Normal Values of Three-Dimensional Right Ventricular Size and Function Measurements: Results of the World Alliance Societies of Echocardiography Study. *J. Am. Soc. Echocardiogr.* **2023**, *36*, 858-866.e1, doi:10.1016/j.echo.2023.04.011.
76. Muresian, H. The Clinical Anatomy of the Right Ventricle. *Clin. Anat.* **2016**, *29*, 380–398, doi:10.1002/ca.22484.
77. Van De Veerdonk, M.C.; Marcus, J.T.; Bogaard, H.; Noordegraaf, A.V. State of the Art: Advanced Imaging of the Right Ventricle and Pulmonary Circulation in Humans (2013 Grover Conference Series). *Pulm. Circ.* **2014**, *4*, 158–168, doi:10.1086/675978.
78. Rudski, L.G.; Lai, W.W.; Afilalo, J.; Hua, L.; Handschumacher, M.D.; Chandrasekaran, K.; Solomon, S.D.; Louie, E.K.; Schiller, N.B. Guidelines for the Echocardiographic Assessment of the Right Heart in Adults:

 doi:10.20944/preprints202505.1456.v1

A Report from the American Society of Echocardiography. *J. Am. Soc. Echocardiogr.* **2010**, *23*, 685–713, doi:10.1016/j.echo.2010.05.010.

79. Rohde, L.E.P.; Montera, M.W.; Bocchi, E.A.; Clausell, N.O.; Albuquerque, D.C.D.; Rassi, S.; Colafranceschi, A.S.; Freitas Junior, A.F.D.; Ferraz, A.S.; Biolo, A.; et al. Diretriz Brasileira de Insuficiência Cardíaca Crônica e Aguda. *Arq. Bras. Cardiol.* **2018**, doi:10.5935/abc.20180190.
80. Hart, C.Y.T.; Meyer, D.M.; Tazelaar, H.D.; Grande, J.P.; Burnett Jr, J.C.; Housmans, P.R.; Redfield, M.M. Load Versus Humoral Activation in the Genesis of Early Hypertensive Heart Disease. *Circulation* **2001**, *104*, 215–220, doi:10.1161/01.CIR.104.2.215.
81. Paulus, W.J.; Tschöpe, C. A Novel Paradigm for Heart Failure With Preserved Ejection Fraction. *J. Am. Coll. Cardiol.* **2013**, *62*, 263–271, doi:10.1016/j.jacc.2013.02.092.
82. Chirinos, J.A.; Segers, P.; Gupta, A.K.; Swillens, A.; Rietzschel, E.R.; De Buyzere, M.L.; Kirkpatrick, J.N.; Gillebert, T.C.; Wang, Y.; Keane, M.G.; et al. Time-Varying Myocardial Stress and Systolic Pressure-Stress Relationship: Role in Myocardial-Arterial Coupling in Hypertension. *Circulation* **2009**, *119*, 2798–2807, doi:10.1161/CIRCULATIONAHA.108.829366.
83. Taube, A.; Schlich, R.; Sell, H.; Eckardt, K.; Eckel, J. Inflammation and Metabolic Dysfunction: Links to Cardiovascular Diseases. *Am. J. Physiol.-Heart Circ. Physiol.* **2012**, *302*, H2148–H2165, doi:10.1152/ajpheart.00907.2011.
84. Van Heerebeek, L.; Hamdani, N.; Falcão-Pires, I.; Leite-Moreira, A.F.; Begieneman, M.P.V.; Bronzwaer, J.G.F.; Van Der Velden, J.; Stienen, G.J.M.; Laarman, G.J.; Somsen, A.; et al. Low Myocardial Protein Kinase G Activity in Heart Failure With Preserved Ejection Fraction. *Circulation* **2012**, *126*, 830–839, doi:10.1161/CIRCULATIONAHA.111.076075.
85. Calderone, A.; Thaik, C.M.; Takahashi, N.; Chang, D.L.; Colucci, W.S. Nitric Oxide, Atrial Natriuretic Peptide, and Cyclic GMP Inhibit the Growth-Promoting Effects of Norepinephrine in Cardiac Myocytes and Fibroblasts. *J. Clin. Invest.* **1998**, *101*, 812–818, doi:10.1172/JCI119883.
86. Takimoto, E.; Champion, H.C.; Li, M.; Belardi, D.; Ren, S.; Rodriguez, E.R.; Bedja, D.; Gabrielson, K.L.; Wang, Y.; Kass, D.A. Chronic Inhibition of Cyclic GMP Phosphodiesterase 5A Prevents and Reverses Cardiac Hypertrophy. *Nat. Med.* **2005**, *11*, 214–222, doi:10.1038/nm1175.
87. Kassis, N.; Layoun, H.; Goyal, A.; Dong, T.; Saad, A.M.; Puri, R.; Griffin, B.P.; Heresi, G.A.; Tonelli, A.R.; Kapadia, S.R.; et al. Mechanistic Insights into Tricuspid Regurgitation Secondary to Pulmonary Arterial Hypertension. *Am. J. Cardiol.* **2022**, *175*, 97–105, doi:10.1016/j.amjcard.2022.04.010.
88. Leach, J.P.; Heallen, T.; Zhang, M.; Rahmani, M.; Morikawa, Y.; Hill, M.C.; Segura, A.; Willerson, J.T.; Martin, J.F. Hippo Pathway Deficiency Reverses Systolic Heart Failure after Infarction. *Nature* **2017**, *550*, 260–264, doi:10.1038/nature24045.
89. Nakada, Y.; Canseco, D.C.; Thet, S.; Abdisalaam, S.; Asaithamby, A.; Santos, C.X.; Shah, A.M.; Zhang, H.; Faber, J.E.; Kinter, M.T.; et al. Hypoxia Induces Heart Regeneration in Adult Mice. *Nature* **2017**, *541*, 222–227, doi:10.1038/nature20173.
90. Van Heerebeek, L.; Paulus, W.J. Understanding Heart Failure with Preserved Ejection Fraction: Where Are We Today? *Neth. Heart J.* **2016**, *24*, 227–236, doi:10.1007/s12471-016-0810-1.
91. Westermann, D.; Lindner, D.; Kasner, M.; Zietsch, C.; Savvatis, K.; Escher, F.; Von Schlippenbach, J.; Skurk, C.; Steendijk, P.; Riad, A.; et al. Cardiac Inflammation Contributes to Changes in the Extracellular Matrix in Patients With Heart Failure and Normal Ejection Fraction. *Circ. Heart Fail.* **2011**, *4*, 44–52, doi:10.1161/CIRCHEARTFAILURE.109.931451.
92. Smith, M.D.; MacPhail, B.; Harrison, M.R.; Lenhoff, S.J.; DeMaria, A.N. Value and Limitations of Transesophageal Echocardiography in Determination of Left Ventricular Volumes and Ejection Fraction. *J. Am. Coll. Cardiol.* **1992**, *19*, 1213–1222, doi:10.1016/0735-1097(92)90327-J.
93. Gottdiener, J.S. Overview of Stress Echocardiography: Uses, Advantages, and Limitations. *Curr. Probl. Cardiol.* **2003**, *28*, 485–516, doi:10.1016/j.cpcardiol.2003.10.001.
94. Saito, Y.; Omae, Y.; Harada, T.; Sorimachi, H.; Yuasa, N.; Kagami, K.; Murakami, F.; Naito, A.; Tani, Y.; Kato, T.; et al. Exercise Stress Echocardiography–Based Phenotyping of Heart Failure With Preserved Ejection Fraction. *J. Am. Soc. Echocardiogr.* **2024**, *37*, 759–768, doi:10.1016/j.echo.2024.05.003.

 doi:10.20944/preprints202505.1456.v1

95. Joffe, S.W.; Ferrara, J.; Chalian, A.; Tighe, D.A.; Aurigemma, G.P.; Goldberg, R.J. Are Ejection Fraction Measurements by Echocardiography and Left Ventriculography Equivalent? *Am. Heart J.* **2009**, *158*, 496–502, doi:10.1016/j.ahj.2009.06.012.
96. Wood, P.W.; Choy, J.B.; Nanda, N.C.; Becher, H. Left Ventricular Ejection Fraction and Volumes: It Depends on the Imaging Method. *Echocardiography* **2014**, *31*, 87–100, doi:10.1111/echo.12331.
97. Harada, T.; Kagami, K.; Kato, T.; Obokata, M. Echocardiography in the Diagnostic Evaluation and Phenotyping of Heart Failure with Preserved Ejection Fraction. *J. Cardiol.* **2022**, *79*, 679–690, doi:10.1016/j.jjcc.2021.11.003.
98. Hotta, V.T.; Rassi, D.D.C.; Pena, J.L.B.; Vieira, M.L.C.; Rodrigues, A.C.T.; Cardoso, J.N.; Ramires, F.J.A.; Nastari, L.; Mady, C.; Fernandes, F. Análise Crítica e Limitações Do Diagnóstico de Insuficiência Cardíaca Com Fração de Ejeção Preservada (ICFEp). *Arq. Bras. Cardiol.* **2022**, doi:10.36660/abc.20210052.
99. Loai, S.; Cheng, H.-L.M. Heart Failure with Preserved Ejection Fraction: The Missing Pieces in Diagnostic Imaging. *Heart Fail. Rev.* **2020**, *25*, 305–319, doi:10.1007/s10741-019-09836-8.
100. Gorcsan, J.; Tanaka, H. Echocardiographic Assessment of Myocardial Strain. *J. Am. Coll. Cardiol.* **2011**, *58*, 1401–1413, doi:10.1016/j.jacc.2011.06.038.
101. Weidemann, F.; Jamal, F.; Sutherland, G.R.; Claus, P.; Kowalski, M.; Hatle, L.; De Scheerder, I.; Bijnens, B.; Rademakers, F.E. Myocardial Function Defined by Strain Rate and Strain during Alterations in Inotropic States and Heart Rate. *Am. J. Physiol.-Heart Circ. Physiol.* **2002**, *283*, H792–H799, doi:10.1152/ajpheart.00025.2002.
102. Voigt, J.-U.; Pedrizzetti, G.; Lysyansky, P.; Marwick, T.H.; Houle, H.; Baumann, R.; Pedri, S.; Ito, Y.; Abe, Y.; Metz, S.; et al. Definitions for a Common Standard for 2D Speckle Tracking Echocardiography: Consensus Document of the EACVI/ASE/Industry Task Force to Standardize Deformation Imaging. *Eur. Heart J. - Cardiovasc. Imaging* **2015**, *16*, 1–11, doi:10.1093/ehjci/jeu184.
103. Smiseth, O.A.; Rider, O.; Cvijic, M.; Valkovič, L.; Remme, E.W.; Voigt, J.-U. Myocardial Strain Imaging. *JACC Cardiovasc. Imaging* **2025**, *18*, 340–381, doi:10.1016/j.jcmg.2024.07.011.
104. Voigt, J.-U.; Cvijic, M. 2- and 3-Dimensional Myocardial Strain in Cardiac Health and Disease. *JACC Cardiovasc. Imaging* **2019**, *12*, 1849–1863, doi:10.1016/j.jcmg.2019.01.044.
105. Bijnens, B.H.; Cikes, M.; Claus, P.; Sutherland, G.R. Velocity and Deformation Imaging for the Assessment of Myocardial Dysfunction. *Eur. J. Echocardiogr.* **2008**, *10*, 216–226, doi:10.1093/ejechocard/jen323.
106. Li, V.W.; So, E.K.; Wong, W.H.; Cheung, Y. Myocardial Deformation Imaging by Speckle-Tracking Echocardiography for Assessment of Cardiotoxicity in Children during and after Chemotherapy: A Systematic Review and Meta-Analysis. *J. Am. Soc. Echocardiogr.* **2022**, *35*, 629–656, doi:10.1016/j.echo.2022.01.017.
107. Collier, P.; Phelan, D.; Klein, A. A Test in Context: Myocardial Strain Measured by Speckle-Tracking Echocardiography. *J. Am. Coll. Cardiol.* **2017**, *69*, 1043–1056, doi:10.1016/j.jacc.2016.12.012.
108. Sitia, S. Speckle Tracking Echocardiography: A New Approach to Myocardial Function. *World J. Cardiol.* **2010**, *2*, 1, doi:10.4330/wjc.v2.i1.1.
109. Acquatella, H. Echocardiography in Chagas Heart Disease. *Circulation* **2007**, *115*, 1124–1131, doi:10.1161/CIRCULATIONAHA.106.627323.
110. Cuddy, S.A.M.; Chetrit, M.; Jankowski, M.; Desai, M.; Falk, R.H.; Weiner, R.B.; Klein, A.L.; Phelan, D.; Grogan, M. Practical Points for Echocardiography in Cardiac Amyloidosis. *J. Am. Soc. Echocardiogr.* **2022**, *35*, A31–A40, doi:10.1016/j.echo.2022.06.006.
111. Little, W.C.; Oh, J.K. Echocardiographic Evaluation of Diastolic Function Can Be Used to Guide Clinical Care. *Circulation* **2009**, *120*, 802–809, doi:10.1161/CIRCULATIONAHA.109.869602.
112. Appleton, C.P.; Hatle, L.K.; Popp, R.L. Relation of Transmitral Flow Velocity Patterns to Left Ventricular Diastolic Function: New Insights from a Combined Hemodynamic and Doppler Echocardiographic Study. *J. Am. Coll. Cardiol.* **1988**, *12*, 426–440, doi:10.1016/0735-1097(88)90416-0.
113. Mulvagh, S.; Quiñones, M.A.; Kleiman, N.S.; Jorge Cheirif, B.; Zoghbi, W.A. Estimation of Left Ventricular End-Diastolic Pressure from Doppler Transmitral Flow Velocity in Cardiac Patients Independent of Systolic Performance. *J. Am. Coll. Cardiol.* **1992**, *20*, 112–119, doi:10.1016/0735-1097(92)90146-E.

 doi:10.20944/preprints202505.1456.v1

114. Appleton, C.P.; Firstenberg, M.S.; Garcia, M.J.; Thomas, J.D. THE ECHO-DOPPLER EVALUATION OF LEFT VENTRICULAR DIASTOLIC FUNCTION. *Cardiol. Clin.* **2000**, *18*, 513–546, doi:10.1016/S0733-8651(05)70159-4.
115. Galderisi, M.; Dini, F.L.; Temporelli, P.L.; Colonna, P.; de Simone, G. [Doppler echocardiography for the assessment of left ventricular diastolic function: methodology, clinical and prognostic value]. *Ital. Heart J. Suppl. Off. J. Ital. Fed. Cardiol.* **2004**, *5*, 86–97.
116. Nagueh, S.F.; Middleton, K.J.; Kopelen, H.A.; Zoghbi, W.A.; Quiñones, M.A. Doppler Tissue Imaging: A Noninvasive Technique for Evaluation of Left Ventricular Relaxation and Estimation of Filling Pressures. *J. Am. Coll. Cardiol.* **1997**, *30*, 1527–1533, doi:10.1016/S0735-1097(97)00344-6.
117. Wang, M.; Yip, G.W.K.; Wang, A.Y.M.; Zhang, Y.; Ho, P.Y.; Tse, M.K.; Lam, P.K.W.; Sanderson, J.E. Peak Early Diastolic Mitral Annulus Velocity by Tissue Doppler Imaging Adds Independent and Incremental Prognostic Value. *J. Am. Coll. Cardiol.* **2003**, *41*, 820–826, doi:10.1016/S0735-1097(02)02921-2.
118. Johnson, N.P.; Gould, K.L.; Di Carli, M.F.; Taqueti, V.R. Invasive FFR and Noninvasive CFR in the Evaluation of Ischemia. *J. Am. Coll. Cardiol.* **2016**, *67*, 2772–2788, doi:10.1016/j.jacc.2016.03.584.
119. Taqueti, V.R.; Shah, A.M.; Everett, B.M.; Pradhan, A.D.; Piazza, G.; Bibbo, C.; Hainer, J.; Morgan, V.; Carolina Do A. H. De Souza, A.; Skali, H.; et al. Coronary Flow Reserve, Inflammation, and Myocardial Strain. *JACC Basic Transl. Sci.* **2023**, *8*, 141–151, doi:10.1016/j.jacbts.2022.08.009.
120. Rush, C.J.; Berry, C.; Oldroyd, K.G.; Rocchiccioli, J.P.; Lindsay, M.M.; Touyz, R.M.; Murphy, C.L.; Ford, T.J.; Sidik, N.; McEntegart, M.B.; et al. Prevalence of Coronary Artery Disease and Coronary Microvascular Dysfunction in Patients With Heart Failure With Preserved Ejection Fraction. *JAMA Cardiol.* **2021**, *6*, 1130, doi:10.1001/jamacardio.2021.1825.
121. Taqueti, V.R.; Di Carli, M.F. Coronary Microvascular Disease Pathogenic Mechanisms and Therapeutic Options. *J. Am. Coll. Cardiol.* **2018**, *72*, 2625–2641, doi:10.1016/j.jacc.2018.09.042.
122. Arnold, J.R.; Kanagala, P.; Budgeon, C.A.; Jerosch-Herold, M.; Gulsin, G.S.; Singh, A.; Khan, J.N.; Chan, D.C.S.; Squire, I.B.; Ng, L.L.; et al. Prevalence and Prognostic Significance of Microvascular Dysfunction in Heart Failure With Preserved Ejection Fraction. *JACC Cardiovasc. Imaging* **2022**, *15*, 1001–1011, doi:10.1016/j.jcmg.2021.11.022.
123. Dryer, K.; Gajjar, M.; Narang, N.; Lee, M.; Paul, J.; Shah, A.P.; Nathan, S.; Butler, J.; Davidson, C.J.; Fearon, W.F.; et al. Coronary Microvascular Dysfunction in Patients with Heart Failure with Preserved Ejection Fraction. *Am. J. Physiol.-Heart Circ. Physiol.* **2018**, *314*, H1033–H1042, doi:10.1152/ajpheart.00680.2017.
124. Mohammed, S.F.; Hussain, S.; Mirzoyev, S.A.; Edwards, W.D.; Maleszewski, J.J.; Redfield, M.M. Coronary Microvascular Rarefaction and Myocardial Fibrosis in Heart Failure With Preserved Ejection Fraction. *Circulation* **2015**, *131*, 550–559, doi:10.1161/CIRCULATIONAHA.114.009625.
125. Berry, C.; Sykes, R. Microvascular Dysfunction in Heart Failure With Preserved Ejection Fraction. *JACC Cardiovasc. Imaging* **2022**, *15*, 1012–1014, doi:10.1016/j.jcmg.2022.04.008.